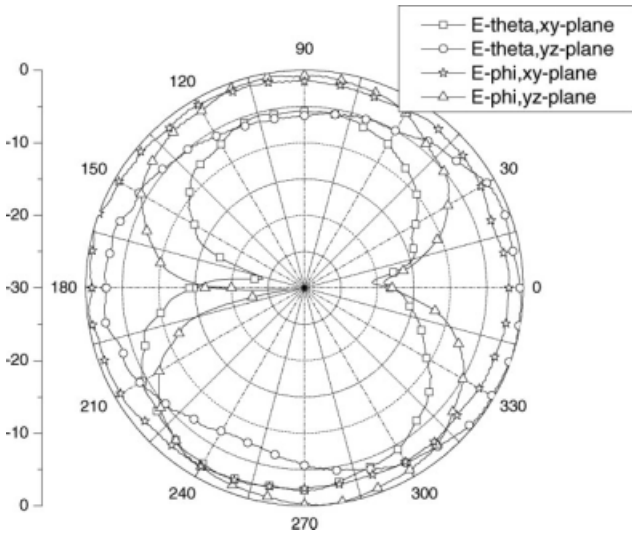

Figure 7 Measured radiation patterns at 2.45 GHz in the *x-y* and *x-z* planes for the antenna

In addition, parametric studies were performed to quantify the effects of height h between the radiation patch and the ground plate of the antenna on S_{11}. From Figure 6, it can be seen that the whole resonant frequency decreases with the increase of h, which owing to the increased equivalent electric length of the antenna.

The radiation pattern of the fabricated antenna was measured at 2.45, 5.2, and 5.75 GHz, which are shown in Figures 7–9, respectively. It can be seen that the radiation patterns at the three resonant frequencies showed omni-directional patterns in the *x-y* plane. At 5.75 GHz, the radiation pattern in the *x-z* plane was not exactly omni-directional; this is due to the effect of the ground plane. The peak gains of the antenna were 1.6 dBi at 2.45 GHz, 2.3 dBi at 5.2 GHz, and 4.4 dBi at 5.75 GHz.

4. CONCLUSIONS

A compact tri-band PIFA for WLAN and WiMAX applications has been proposed and the effects of dimensions have been studied. By using the F-T-shaped slots in the radiation patch and introducing trapezoidal feeding plate, the three resonant modes are generated. The size of the fabricated radiation patch and ground plane are $25 \times 11 \times 8$ mm^3 and 26×40 mm^2; this is much smaller than a conventional inverted-F antenna. Because of its nearly omni-directional radiation pattern, the antenna has wide and potential applications for wireless communication applications.

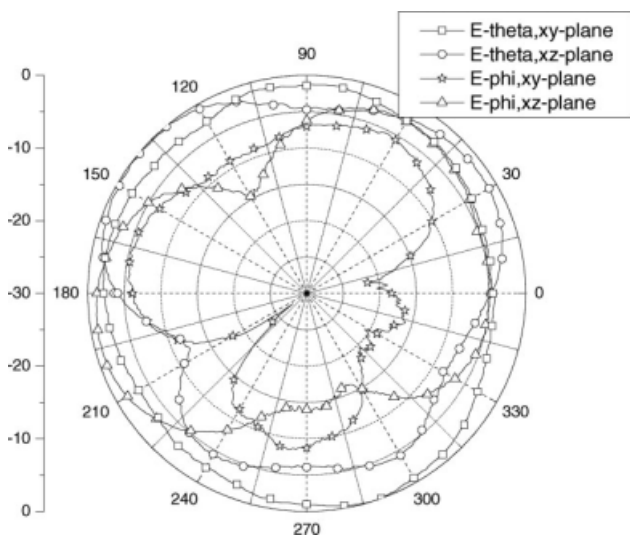

Figure 8 Measured radiation patterns at 5.2 GHz in the *x-y* and *x-z* planes for the antenna

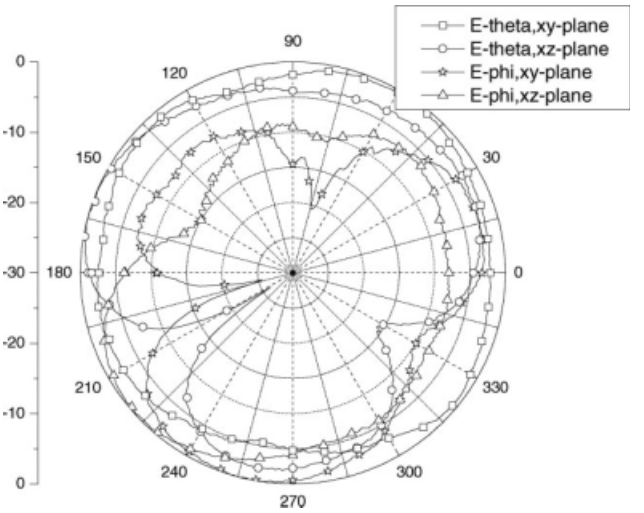

Figure 9 Measured radiation patterns at 5.75 GHz in the *x-y* and *x-z* planes for the antenna

REFERENCES

1. P. Nepa, G. Manara, A.A. Serra, and G. Nenna, Multiband PIFA for WLAN mobile terminals, IEEE Antennas Wireless Propag Lett 4 (2005).
2. F. Wang, A. Ghosh, C. Sankaran, P.J. Fleming, F. Hsieh, and S.J. Benes, Mobile WiMAX systems: Performance and evolution. IEEE Commun Mag (2008).
3. Y.J. Cho, Y.S. Shin, and S.O. Park, Internal PIFA for 2.4/5 GHz WLAN applications, Electron Lett 42 (2006).
4. C.-Y.-D. Sim and S.-Y. Tu, Dual-frequency shorted patch antenna for WLAN applications, Microwave Opt Technol Lett 49 (2007).
5. P. Salonen, M. Keskilammi, and M. Kivikoski, Single-feed dual-band planar inverted-F antenna with U-shaped slot, IEEE Trans Antennas Propag 48 (2000), 1262–1264.
6. R. Feick, H. Carrasco, M. Olmos, and H.D. Hristov, PIFA input bandwidth enhancement by changing feed plate silhouette, Electron Lett 40 (2004), 921–922.

INTERNAL WIRELESS WIDE AREA NETWORK CLAMSHELL MOBILE PHONE ANTENNA WITH REDUCED GROUND PLANE EFFECTS

Wei-Yu Li and Kin-Lu Wong
Department of Electrical Engineering, National Sun Yat-sen University, Kaohsiung 80424, Taiwan, Republic of China;
Corresponding author: wongkl@ema.ee.nsysu.edu.tw

Received 20 June 2009

ABSTRACT: *An internal wireless wide area network (WWAN) antenna applied in a clamshell mobile phone having an equivalent band-stop circuit at the hinge to decrease the upper ground plane effects of the mobile phone on the antenna performances is presented. The internal*

WWAN antenna in this study is a small-size printed monopole mounted at the bottom of the main ground. This band-stop circuit can perform a parallel resonance at around 900 MHz and leads to high impedance seen into the upper ground in the 900 MHz band, which greatly decreases the excited surface currents on the upper ground. At around 1900 MHz, owing to its shorter wavelength, the surface currents on the upper ground excited by the internal antenna on the main ground are small for both the traditional and proposed clamshell mobile phone structures. Hence, over the WWAN operating bands, the presence of the upper ground shows very small effects on the impedance matching and radiation characteristics of the antenna on the main ground. The SAR and HAC studies on the proposed clamshell mobile phone structure are also presented. © 2010 Wiley Periodicals, Inc. Microwave Opt Technol Lett 52: 922–930, 2010; Published online in Wiley InterScience (www.interscience.wiley.com). DOI 10.1002/mop.25056

Key words: *handset antennas; WWAN antennas; clamshell mobile phone antennas; reduced ground plane effects; band-stop circuit*

1. INTRODUCTION

For internal wireless wide area network (WWAN) antennas applied in the clamshell mobile phone, where there are two (upper and main) ground planes, different from that of the bar-type mobile phones, the antenna performances usually suffer large effects from the presence of the upper ground plane and its different orientations to the main ground plane for the open state (talk condition) and closed state (idle condition) [1–11]. This upper ground plane effect is usually significant for the antenna's lower band at about 900 MHz. However, there are very few related studies in the published articles. The upper ground plane effect is still a challenging problem for the design of the internal WWAN antenna in the clamshell mobile phone.

To suppress or decrease the upper ground plane effects on the performances of the internal WWAN antenna, we propose in this article to introduce an equivalent band-stop circuit [12, 13] formed by distributed elements at the hinge of the clamshell mobile phone to create a parallel resonance at about 900 MHz, which results in high impedance seen at the hinge into the upper ground plane for the 900 MHz band. This proposed design is related to the idea proposed in [7, 14] in which however, no detailed results are presented. With the parallel resonance created at the hinge, the excited surface currents on the upper ground plane caused by the internal antenna mounted at the main ground plane will be greatly decreased. This behavior can result in decreased effect of the upper ground plane on the performances of the internal WWAN antenna.

With the proposed equivalent band-stop circuit to achieve reduced ground plane effect, different orientations of the upper ground plane to the main ground plane such as the clamshell

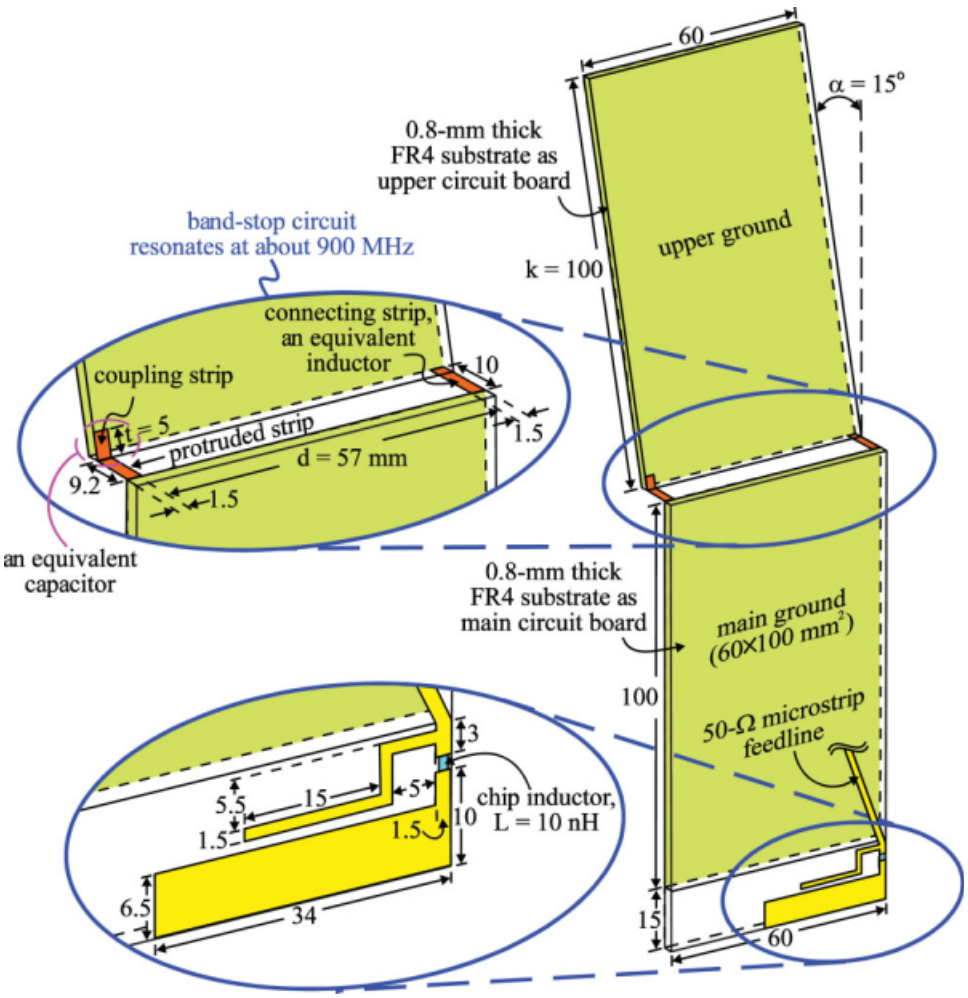

Figure 1 Proposed structure of an internal printed penta-band WWAN antenna placed at the bottom of the main circuit board and an equivalent band-stop circuit at the hinge of the clamshell mobile phone. [Color figure can be viewed in the online issue, which is available at www.interscience.wiley.com]

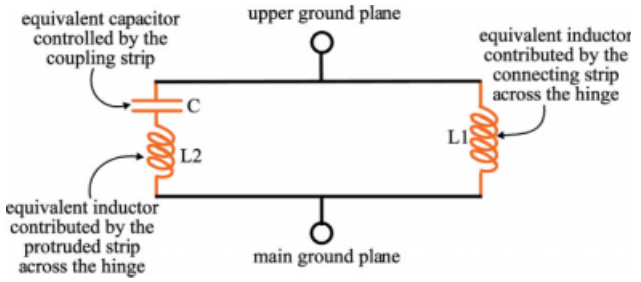

Figure 2 Equivalent band-stop circuit at the hinge of the clamshell mobile phone. [Color figure can be viewed in the online issue, which is available at www.interscience.wiley.com]

mobile phone in the open and closed states will cause small variations on the performances of the internal WWAN antenna for GSM850/900/1800/1900/UMTS operation. Further, the proposed design can cause decreased excited surface currents on the upper ground plane on which the acoustic output is located and is usually attached onto the user's ear in the open state for the talk condition, hence resulting in weaker strengths of the near-field electric fields in the vicinity of the upper ground plane. This can result in decreased hearing aid compatibility (HAC) and specific absorption rate (SAR) values, making it easy for the mobile phone to meet the HAC standard ANSI C63.19-2007 [15] and the SAR limit of 1.6 W/kg for the 1-g head tissue and 2.0 W/kg for the 10-g head tissue [16, 17]. Details of the proposed structure for reduced ground plane effects in the clamshell mobile phone are presented and discussed.

2. PROPOSED STRUCTURE FOR REDUCED GROUND PLANE EFFECTS

Figure 1 shows the proposed structure of an internal clamshell mobile phone antenna placed at the bottom of the main circuit board and an equivalent band-stop circuit at the hinge of the mobile phone. The internal antenna studied here is a printed penta-band WWAN antenna capable of covering GSM850/900/1800/1900/UMTS (824~894/890~960/1710~1880/1850~1990/1920~2170 MHz) bands in the bar-type mobile phone [18]. The antenna consists of a chip-inductor-embedded longer radiating strip and a shorter radiating strip. With a 10-nH chip inductor embedded, the longer radiating strip has a length of about 46 mm only, yet supporting a wide resonant mode at about 900 MHz for GSM850/900 operation. For the shorter radiating strip, it has a length of about 30 mm and provides a wide resonant mode at about 1900 MHz for GSM1800/1900/UMTS operation. This penta-band strip monopole antenna occupies a small area of about 350 mm^2 on the main circuit board and is selected in this study to be applied in the proposed clamshell mobile phone structure having an equivalent band-stop circuit at the hinge of the mobile phone. It will be demonstrated in this study that with the same design dimensions as in [18] for the bar-type mobile phone, this internal penta-band strip monopole antenna in the proposed clamshell mobile phone structure shows similar

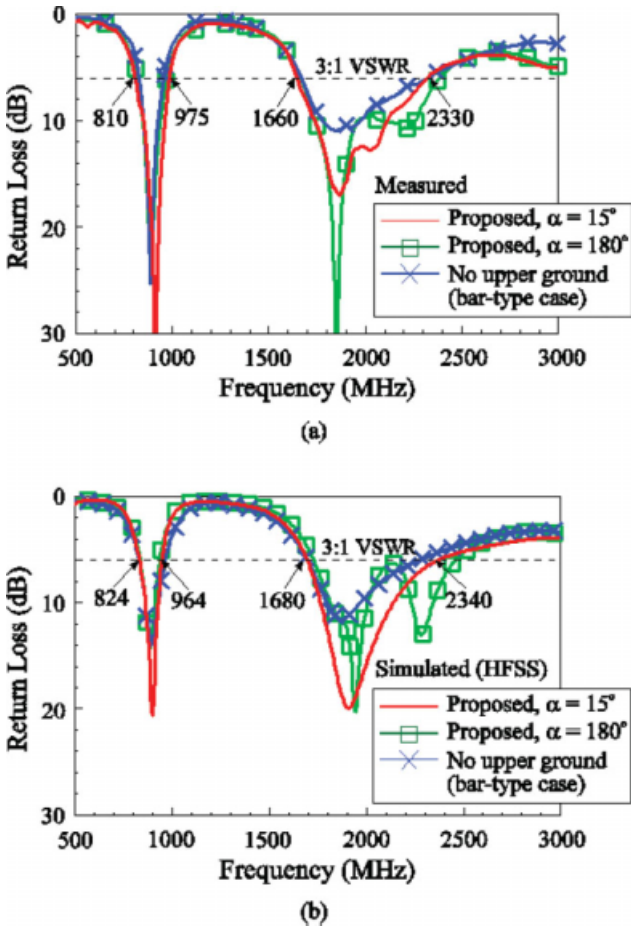

Figure 3 (a) Measured and (b) simulated return loss for the antenna in the open state ($\alpha = 15°$) and closed state ($\alpha = 180°$) of the clamshell mobile phone and in the case of no upper ground plane (i.e., a bar-type mobile phone). [Color figure can be viewed in the online issue, which is available at www.interscience.wiley.com]

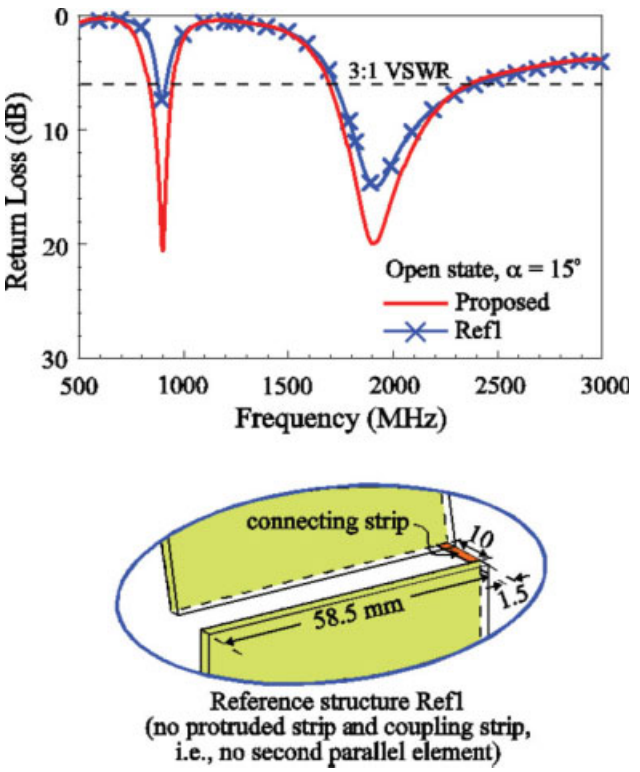

Figure 4 Simulated return loss for the antenna in the proposed structure and reference structure Ref1 [no second parallel element (protruded strip and coupling strip)]. [Color figure can be viewed in the online issue, which is available at www.interscience.wiley.com]

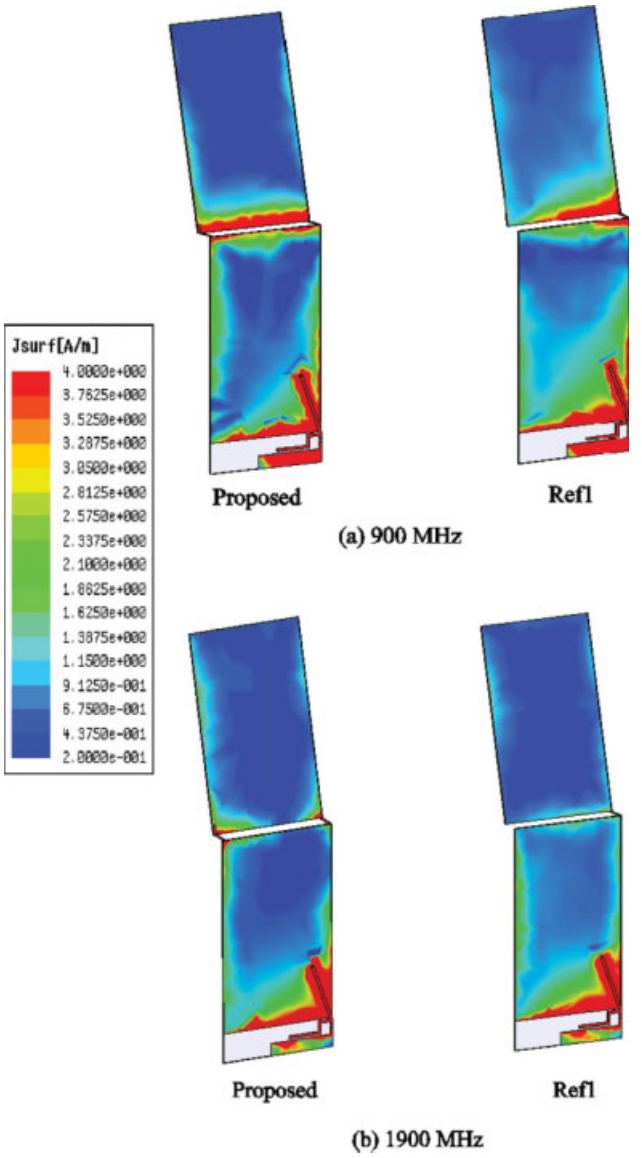

Figure 5 Simulated surface current distributions for the proposed structure and reference structure (Ref1 in Fig. 4) in the open state at (a) 900 MHz and (b) 1900 MHz. [Color figure can be viewed in the online issue, which is available at www.interscience.wiley.com]

impedance matching and radiation performances as obtained in [18]. That is, the presence of the upper ground plane and its different orientations (such as the open state for the talk condition and the closed state for the idle condition) to the main ground plane show small effects on the studied internal WWAN antenna in the clamshell mobile phone.

In the study, the two (main and upper) ground planes of the clamshell mobile phone have the same dimensions of 60×100 mm^2, and the upper ground plane is oriented to the main ground plane with an angle of 15° (α) as shown in Figure 1 for the open state (talk condition). In the closed state (idle condition), the upper ground plane will be parallel to the main ground plane with $\alpha = 180°$. Also note that the main ground plane is printed on a 0.8-mm thick FR4 substrate, which is treated as the main circuit board of the clamshell mobile phone, whereas the upper ground plane is also printed on a 0.8-mm thick FR4 substrate and considered as the upper circuit board of the clamshell mobile phone.

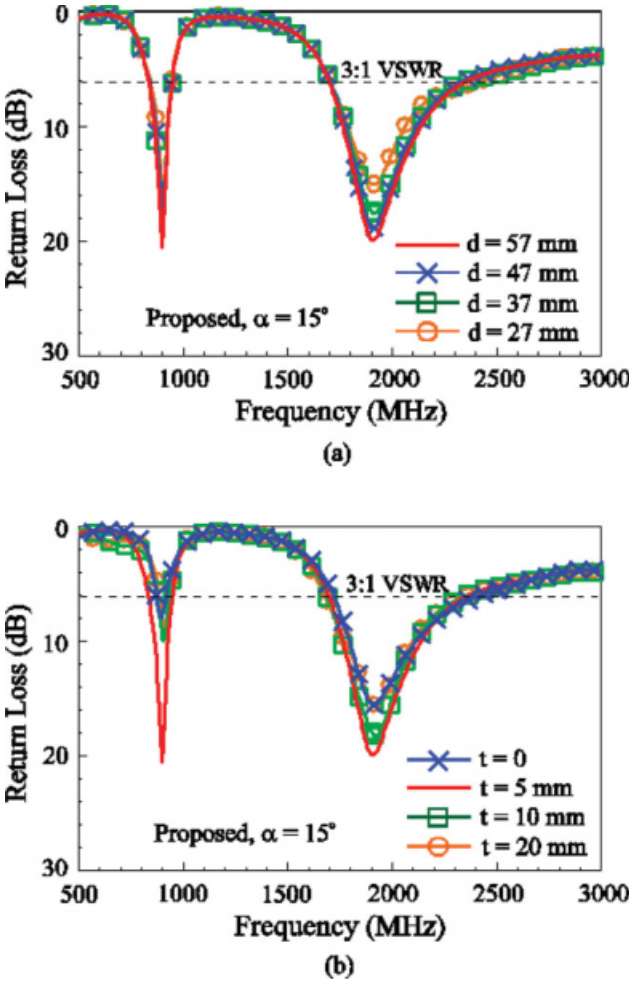

Figure 6 Simulated return loss as a function of (a) the distance d between the two parallel elements and (b) the length t of the coupling strip. Other dimensions are the same as given in Figure 1. [Color figure can be viewed in the online issue, which is available at www.interscience.wiley.com]

The equivalent band-stop circuit at the hinge of the mobile phone is formed by two parallel distributed elements. The first element is a connecting strip (width 1.5 mm and length 10 mm)

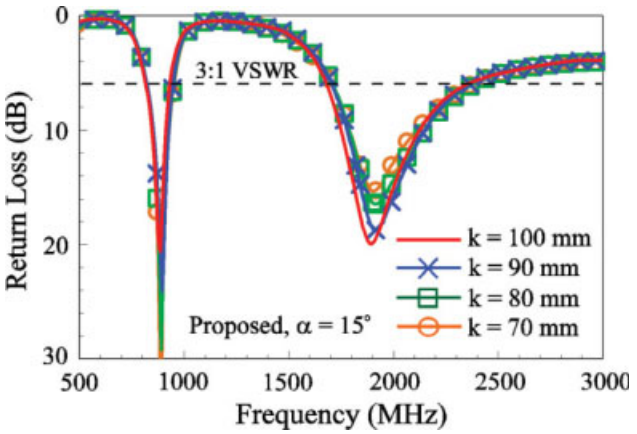

Figure 7 Simulated return loss as a function of the length k of the upper ground plane. Other dimensions are the same as given in Figure 1. [Color figure can be viewed in the online issue, which is available at www.interscience.wiley.com]

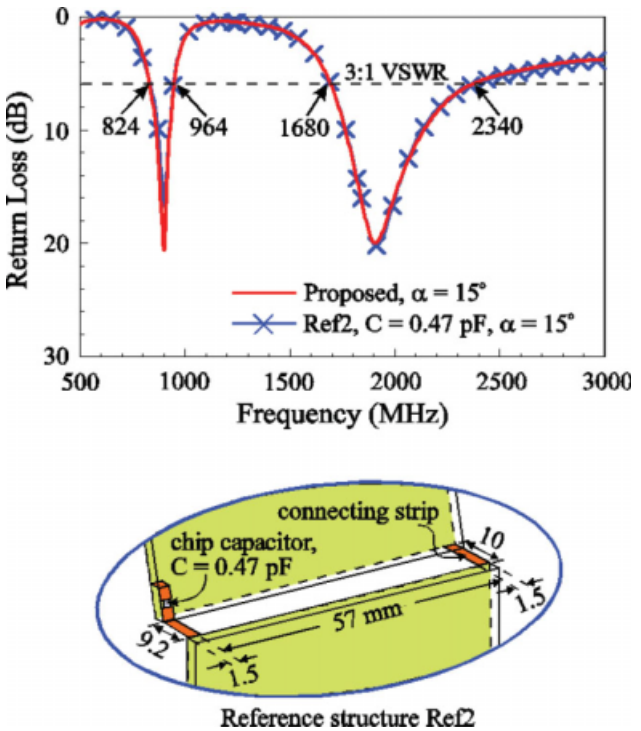

Figure 8 Simulated return loss for the proposed structure and reference structure Ref2 (a chip capacitor of 0.47 pF replacing the coupling strip). [Color figure can be viewed in the online issue, which is available at www.interscience.wiley.com]

across the hinge to connect the two ground planes; this element functions as a distributed inductor in the equivalent circuit shown in Figure 2. The second element comprises a metal strip (width 1.5 mm and length 9.2 mm) protruded from the main ground plane and across the hinge connecting to a coupling strip (length $t = 5$ mm and width 1.5 mm), which capacitively couples to the upper ground plane through the 0.8-mm thick FR4 substrate; this element functions as a distributed inductor in series with an equivalent capacitor as shown in Figure 2. The distance d between the two elements is 57 mm; however, the distance t can be varied with very small effects on the performances of the internal WWAN antenna. The equivalent capacitor in the second element can also be replaced by using a chip capacitor of 4.7 pF (the inset in Fig. 8), hence the antenna performances is almost not affected.

The proposed band-stop circuit at the hinge of the mobile phone is designed to result in a parallel resonance at around 900 MHz. This leads to high impedance seen into the upper ground plane in the 900 MHz band and greatly decreases the possible surface currents excited on the upper ground plane by the internal antenna mounted at the bottom of the main circuit board. In this case, the effects of the upper ground plane on the performances of the internal antenna in the 900 MHz band are greatly reduced. For operating in the antenna's upper band at around 1900 MHz covering GSM1800/1900/UMTS operation, the wavelengths of the operating frequencies are much shorter than those in the 900 MHz band, and hence the excited surface currents are relatively much weaker on upper ground plane, owing to its much larger size seen by the internal antenna at around 1900 MHz. That is, the upper ground plane effects are

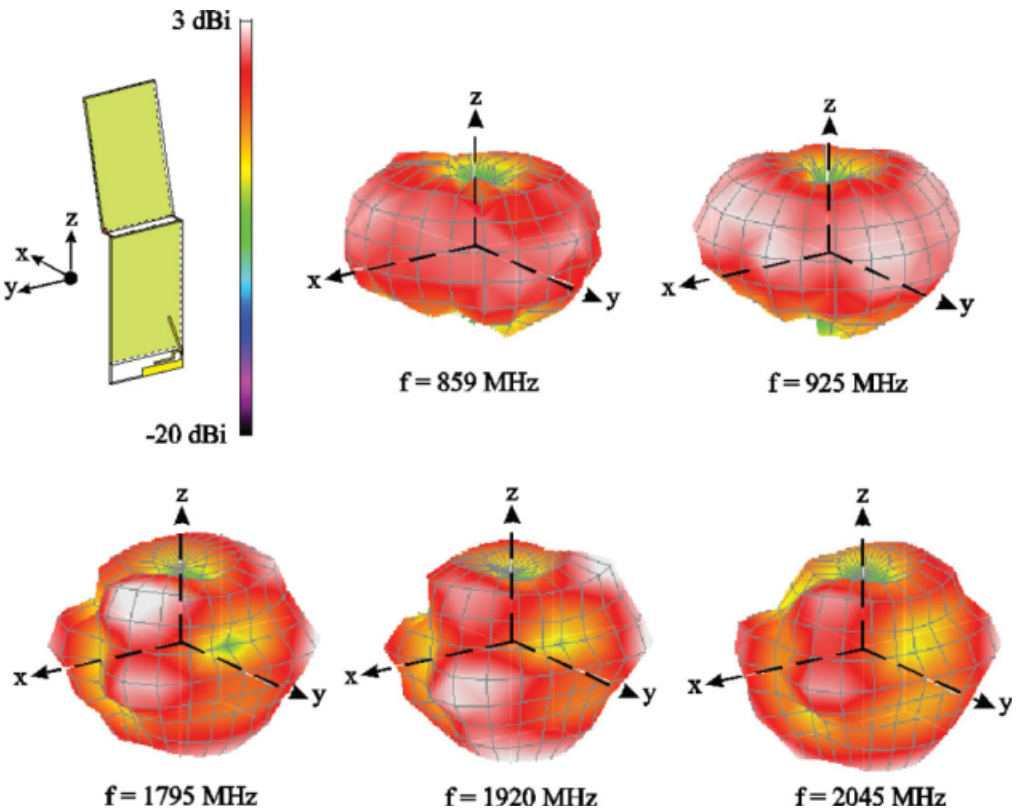

Figure 9 Measured three-dimensional (3-D) radiation patterns for the antenna in the proposed structure with $\alpha = 15°$. [Color figure can be viewed in the online issue, which is available at www.interscience.wiley.com]

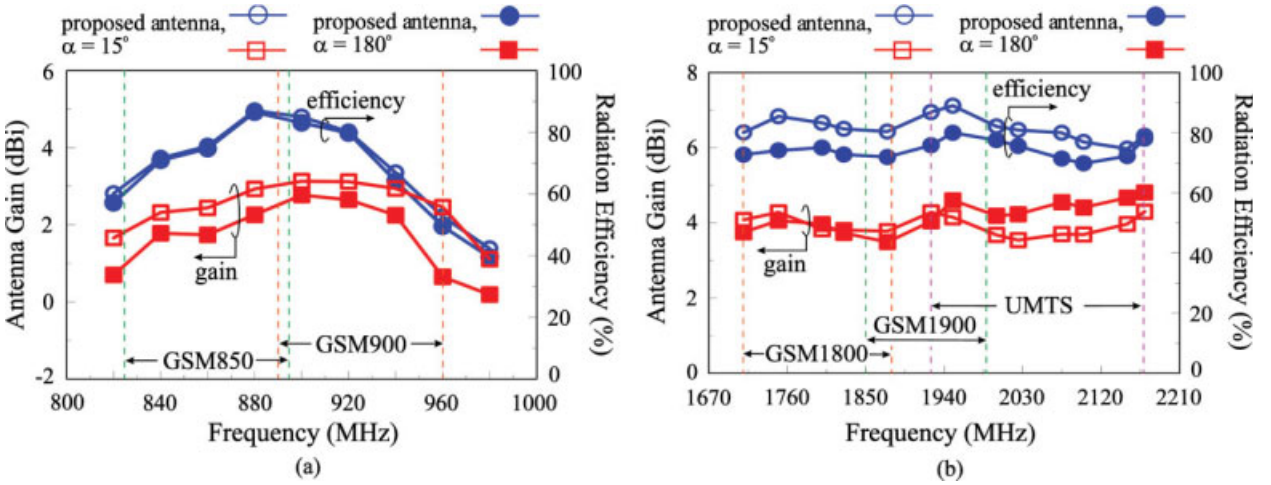

Figure 10 Measured radiation efficiency and antenna gain for the antenna in the open state ($\alpha = 15°$) and closed state ($\alpha = 180°$) of the clamshell mobile phone. (a) The GSM850/900 bands. (b) The GSM1800/1900/UMTS bands. [Color figure can be viewed in the online issue, which is available at www.interscience.wiley.com]

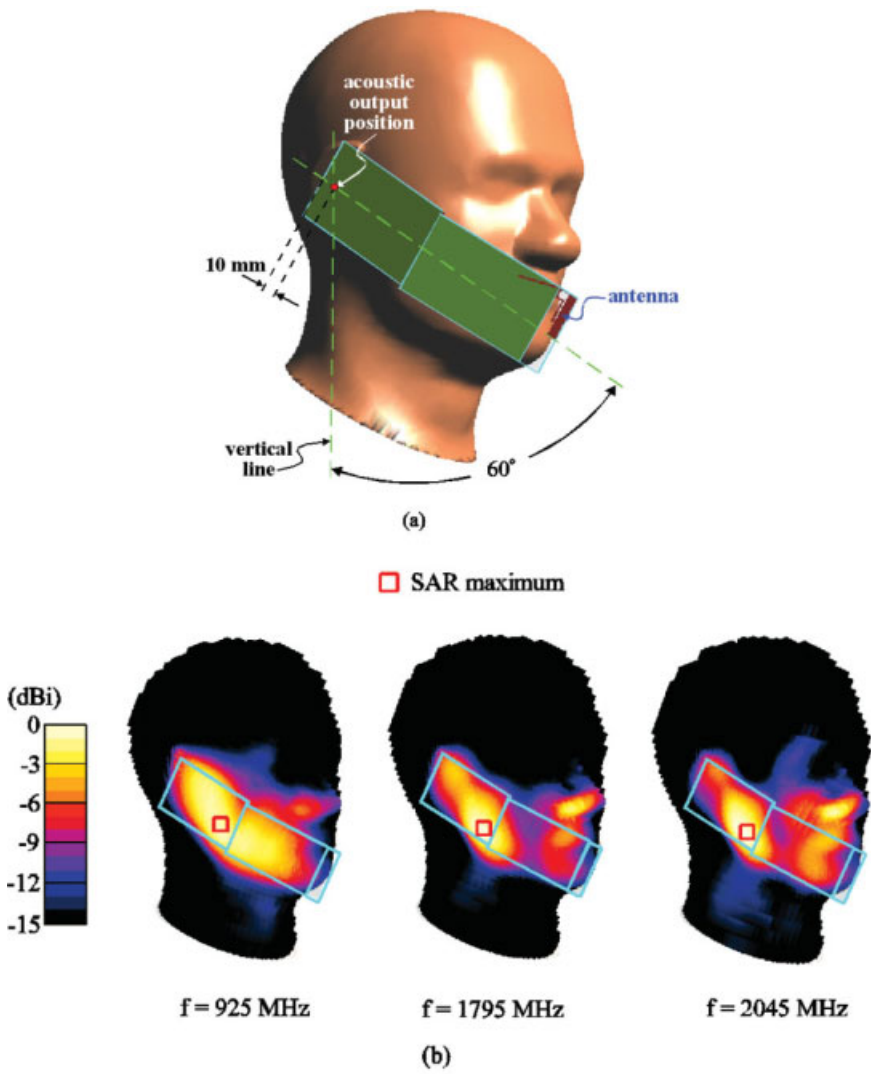

Figure 11 (a) SAR simulation model provided by SEMCAD. (b) Simulated SAR distributions for 1-g head tissue on the phantom head at 925, 1795 and 2045 MHz. [Color figure can be viewed in the online issue, which is available at www.interscience.wiley.com]

small on the upper band of the internal antenna for the traditional clamshell mobile phone [that is, the second parallel element at the hinge is not present (the inset in Fig. 4)]. The proposed band-stop circuit at the hinge also shows small effects on the upper band of the internal antenna. Hence, over the five operating bands for WWAN operation, the presence of the upper ground plane and its different orientations to the main ground plane shows small effects on the performances of the internal antenna in the proposed clamshell mobile phone with the band-stop circuit at the hinge. Detailed results of the equivalent band-stop circuit at the hinge of the clamshell mobile phone are presented and analyzed in the next section.

3. RESULTS AND DISCUSSION

Figure 3(a) shows the measured return loss for the antenna in the open state ($\alpha = 15^\circ$) and closed state ($\alpha = 180^\circ$) of the clamshell mobile phone and in the case of no upper ground plane (i.e., a bar-type mobile phone). The measured data generally agree with the simulated results obtained using Ansoft HFSS [19] shown in Figure 3(b). From the results, two wide operating bands at about 900 and 1900 MHz are obtained. Further, the obtained bandwidths of the antenna's lower and upper bands for the three cases shown in the figure are about the same. The lower band covers GSM850/900 operation, while the upper band covers GSM1800/1900/UMTS operation. The results clearly indicate that the effects of the upper ground plane on the antenna performances are small for the internal WWAN antenna in the proposed clamshell mobile phone structure.

Figure 4 shows the simulated return loss for the antenna in the proposed structure and the reference structure Ref1 where there is no second parallel element (protruded strip and coupling strip) at the hinge. In the Ref1 structure, large effects in the antenna's lower band are seen; the impedance matching for frequencies in the 900 MHz band is quickly degraded when the second parallel element is not present. Whereas for the antenna's upper band at about 1900 MHz, small variations in the impedance matching are seen. This behavior agrees with the discussion in Section II, which is because of the much smaller wavelengths of the operating frequencies in the 1900 MHz band much shorter than those in the 900 MHz band, making the effective size of the upper ground plane much larger at about 1900 MHz. Thus, the excited surface currents are relatively much weaker on the upper ground plane in the 1900 MHz band, thereby resulting in small upper ground plane effects on the internal WWAN antenna studied here.

The simulated surface current distributions for the proposed structure and reference structure (Ref1 in Fig. 4) in the open state at 900 and 1900 MHz are also presented in Figure 5 for comparison. For the results at 900 MHz shown in Figure 5(a), large surface currents at the hinge of the mobile phone are seen, which is owing to the parallel resonance generated by the equivalent band-stop circuit at the hinge. The surface currents on the upper ground plane of the proposed structure are also seen to be greatly decreased compared to those on the upper ground plane of the Ref1 structure. This agrees with the observation in Figure 3 that the upper ground plane effects for the proposed structure are small. For the results at 1900 MHz shown in Figure 5(b), the surface currents on the upper ground plane are much weaker than those on the main ground plane for both the proposed and the Ref1 structures. This also explains the small upper ground plane effects seen in the antenna's upper band in this study.

A parametric study on the equivalent band-stop circuit at the hinge is also conducted. Figure 6(a) shows the simulated return loss as a function of the distance d between the two parallel elements in the band-stop circuit. Other dimensions are the same as given in Figure 1. Results for the distance d varied from 27 to 57 mm are shown. In the study, the first parallel element (the connecting strip) is fixed at one corner, while the second parallel element is moved from the other corner towards the first element. Results show that very small effects are seen for various distances of d. On the other hand, when the length t of the coupling strip in the second parallel element is varied, large effects in the antenna's lower band are observed. Results for the length t varied from 0 to 20 mm are presented in Figure 6(b). The distance d is fixed as 57 mm and other parameters are also the same as in Figure 1. The observed results are reasonable, because the coupling strip contributes the series equivalent capacitor in the second parallel element and the variations in the length t will result in variations in the equivalent capacitance contributed by the coupling strip.

Effects of the length k of the upper ground plane are analyzed in Figure 7 in which the simulated return loss for the length k varied from 70 to 100 mm are shown. Very small variations are seen in the impedance matching over the antenna's lower and upper bands. This behavior is also related to the much weaker surface currents observed in the upper ground plane, especially in the portions near the open edge of the upper ground plane (Fig. 5). It is also interesting to see that the coupling strip can be replaced by a chip capacitor of 0.47 pF (reference structure Ref2 in the inset of Fig. 8). In this case, from the results shown in Figure 8, the simulated return loss for the proposed structure and the Ref2 structure is generally the same.

Figure 9 plots the measured three-dimensional (3-D) radiation patterns for the antenna in the proposed structure with $\alpha = 15^\circ$ (the open state). Dipole-like radiation patterns with omnidirectional radiation in the azimuthal plane (x-y plane) at 859 and 925 MHz are observed. For 1795, 1920, and 2045 MHz in the upper band, the measured radiation patterns are generally about the same, although there are more variations compared to those at 859 and 925 MHz. From the results, the stable radiation patterns over the antenna's lower and upper bands are obtained. Figure 10 shows the measured radiation efficiency and antenna gain for the antenna in the open state ($\alpha = 15^\circ$) and closed state ($\alpha = 180^\circ$) of the clamshell mobile phone. Over the GSM850/900 bands shown in Figure 10(a), the radiation efficiency is about the same for the two different operating states and is varied from about 50 to 87%. For the antenna gain in the open state, it is ranged from about 1.8 to 3.1 dBi over the GSM850/900 bands. In the closed state, the antenna gain is decreased by about 1 dB, which is mainly owing to the variations in the radiation patterns in the two different states. Over the GSM1800/1900/UMTS bands shown in Figure 10(b), the radiation efficiency in the open state is ranged from about 75% to 89%. When the antenna is in the closed state, a small decrease of about or less than 10% in the radiation efficiency is seen. For

TABLE 1 Parameters of the Simulation Phantom Model Studied in Figure 11

	GSM850/900 Bands		GSM1800/1900/UMTS Bands	
	ε_r	σ (S/m)	ε_r	σ (S/m)
Head liquid	41.5	0.97	40	1.4
Head shell	3.5	0	3.5	0

TABLE 2 Simulated SAR (SEMCAD) for the Proposed Structure Studied in Figure 11

	Frequency (Return Loss at the Testing Frequency)				
(W/kg)	859 MHz (13.8 dB)	925 MHz (12.4 dB)	1795 MHz (10.6 dB)	1920 MHz (15.0 dB)	2045 MHz (10.6 dB)
1-g SAR	0.45	0.49	0.25	0.23	0.18
10-g SAR	0.34	0.38	0.16	0.14	0.11

The input power is 24 dBm at 859 and 925 MHz, and 21 dBm at 1795, 1920, and 2045 MHz [21].

the antenna gain in the open state, it is varied in a small range of about 3.5–4.3 dBi. Some variations in the antenna gain are also seen for the two different states, which is again owing to the variations in the radiation patterns caused by the different orientations of the upper ground plane to the main ground plane.

4. SAR AND HAC STUDIES

For practical applications, the SAR and HAC (required for the U.S. market [15]) should be analyzed. For the SAR result, it should meet the limit of 1.6 W/kg for the 1-g head tissue or 2.0 W/kg for the 10-g head tissue. Figure 11(a) shows the SAR simulation model provided by SEMCAD [20], and the parameters of the simulation phantom model are listed in Table 1. The simulated SAR values at the central frequencies of the five operating bands are given in Table 2. The corresponding simulated SAR distributions for 1-g head tissue on the phantom head at 925, 1795, and 2045 MHz are shown in Figure 11(b). In the study, the acoustic output position at the upper ground plane [Fig. 11(a)] is placed close to the phantom ear with a distance of 3 mm. The obtained 1-g SAR values are lower than 0.5 W/kg for all the tested frequencies and good impedance matching is maintained for the proposed antenna with the presence of the phantom head (Table 2). For the 10-g SAR values, they are all lower than 0.4 W/kg. The obtained SAR values are well below the limit for practical applications.

The HAC is tested based on the standard ANSI C63.19-2007 [15]. Figure 12 shows the HAC simulation model provided by SEMCAD complying with the standard ANSI C63.19-2007. The observation plane divided into nine cells has a size of 50 × 50 mm^2 and is centered 15 mm above the acoustic output of 3 mm here. The HAC values are determined from the peak E-field and H-field strengths among the nine cells by excluding three consecutive cells having the strongest field strengths along the boundary of the observation plane. The obtained HAC results are shown in Table 3. In the study, the input power is 33 dBm (2 W continuous input power) at 859 and 925 MHz, 30 dBm at 1795 and 1920 MHz (1 W continuous input power), and 21 dBm (0.125 W continuous input power). From the results shown, the

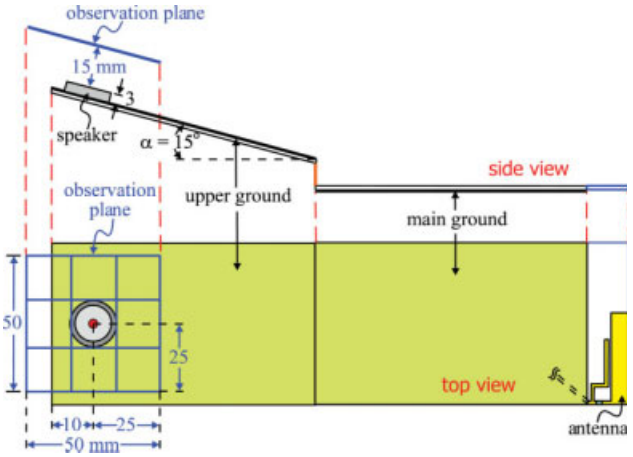

Figure 12 HAC simulation model provided by SEMCAD complying with the standard ANSI C63.19-2007 [15]. [Color figure can be viewed in the online issue, which is available at www.interscience.wiley.com]

E-field and H-field strengths at 859 MHz are 45.1 dBV/m and −9.7 dBA/m, respectively; in this case, it is rated in the M3 Category [22–24]. Similarly, the near-field strengths at 925, 1795, and 1920 MHz are also rated in the M3 category, whereas those at 2045 MHz are rated in the M4 category. With all rated at least in the M3 category, the proposed clamshell mobile phone structure can be treated as a hearing-aid compatible communication device meeting ANSI C63.19-2007 [15].

5. CONCLUSIONS

A clamshell mobile phone structure having an equivalent band-stop circuit at the hinge to achieve reduced upper ground plane effects on its internal WWAN antenna has been proposed and studied. The band-stop circuit formed by two parallel distributed elements across the hinge of the mobile phone can generate a parallel resonance at about 900 MHz. The proposed clamshell mobile phone structure can hence have much decreased surface currents excited on the upper ground plane, when compared to the traditional clamshell mobile phone structure. This behavior results in decreased upper ground plane effects on the performances of the internal WWAN antenna applied in the proposed clamshell mobile phone structure, and good radiation characteristics for the clamshell mobile phone in the open and the closed states have been obtained. Further, owing to the decreased surface currents on the upper ground plane, the near-field electric and magnetic fields are also expected to be smaller. Thus, the obtained SAR values for both the 1-g and 10-g head tissues have been found to be well below the limit for practical applications. The proposed clamshell mobile phone has also been

TABLE 3 Simulated Results (SEMCAD) of Peak Electric- and Magnetic-Field Strengths for the Proposed Structure on the Observation Plane Studied in Figure 12

	Frequency (MHz)				
Peak Field Strength	859	925	1795	1920	2045
E-field (V/m)	179 (45.1 dB)	189 (45.5 dB)	82.4 (38.3 dB)	74.7 (37.5 dB)	19.3 (25.7 dB)
E-field category	M3	M3	M3	M3	M4
H-field (A/m)	0.327 (−9.7 dB)	0.367 (−8.7 dB)	0.247 (−12.1 dB)	0.23 (−12.8 dB)	0.06 (−24.4 dB)
H-field category	M4	M4	M3	M3	M4

evaluated to meet the HAC standard and can be treated as a hearing-aid compatible communication device.

REFERENCES

1. T. Sugiyama, H. Horita, Y. Shirakawa, M. Ikegaya, S. Takaba, and H. Tate, Triple-band internal antenna for clamshell type mobile phone, Hitachi Cable Rev (2003), 26–31
2. P.L. Teng, T.W. Chiou, and K.L. Wong, Internal planar monopole antenna for GSM/DCS/PCS folder-type mobile phone, Microwave Opt Technol Lett 39 (2003), 106–108.
3. K.L. Wong, S.W. Su, C.L. Tang, and S.H. Yeh, Internal shorted patch antenna for a UMTS folder-type mobile phone, IEEE Trans Antennas Propag 53 (2005), 3391–3394.
4. K.L. Wong, W.C. Su, and F.S. Chang, Wideband internal folded planar monopole antenna for UMTS/WiMAX folder-type mobile phone, Microwave Opt Technol Lett 48 (2006), 324–327.
5. K.L. Wong, Y.W. Chi, B. Chen, and S. Yang, Internal DTV antenna for folder-type mobile phone, Microwave Opt Technol Lett 48 (2006), 1015–1019.
6. M. Tzortzakakis and R.J. Langley, Quad-band internal mobile phone antenna, IEEE Trans Antennas Propag 55 (2007), 2097–2103.
7. B.S. Collins, Improving the RF performance of clamshell handsets, In: Proceedings of IEEE International Workshop on Antenna Technology: Small Antennas and Metamaterials, 2006, pp. 265–268.
8. C.I. Lin and K.L. Wong, Printed monopole slot antenna for penta-band operation in the folder-type mobile phone, Microwave Opt Technol Lett 50 (2008), 2237–2241.
9. K.L. Wong and S.Y. Tu, Ultra-wideband coupled-fed loop antenna for penta-band folder-type mobile phone, Microwave Opt Technol Lett 50 (2008), 2706–2712.
10. C.H. Chang, K.L. Wong, and J.S. Row, Coupled-fed small-size PIFA for penta-band folder-type mobile phone application, Microwave Opt Technol Lett 51 (2009), 18–23.
11. C.H. Wu and K.L. Wong, Ultra-wideband PIFA with a capacitive feed for penta-band folder-type mobile phone antenna, IEEE Trans Antennas Propag 57 (2009), 2461–2464.
12. Y.W. Chi and K.L. Wong, Very-small-size folded loop antenna with a band-stop matching circuit for WWAN operation in the mobile phone, Microwave Opt Technol Lett 51 (2009), 808–814.
13. R. Ludwig and P. Bretchko, RF circuit design theory and applications, Prentice-Hall, New Jersey, 2000.
14. H. Liu, A. Napoles, and B.O. White, Wireless device with distributed load, U.S. Patent No. 7,199,762 B2, April 3, 2007.
15. American National Standards Institute, American National Standard for method of measurement of compatibility between wireless communication devices and hearing aids, ANSI C63.19-2007, revision ANSI C63.19-2006, American National Standards Institute, New York, 2007.
16. American National Standards Institute (ANSI), Safety levels with respect to human exposure to radio-frequency electromagnetic field, 3 kHz to 300 GHz, ANSI/IEEE standard C95.1, 1999.
17. J.C. Lin, Specific absorption rates induced in head tissues by microwave radiation from cell phones, Microwave (2001), 22–25.
18. T.W. Kang and K.L. Wong, Chip-inductor-embedded small-size printed strip monopole for WWAN operation in the mobile phone, Microwave Opt Technol Lett 51 (2009), 966–971.
19. http://www.ansoft.com/products/hf/hfss/. This is the official web site of the Ansoft Corporation HFSS.
20. http://www.semcad.com. This is the official web site of the SEMCAD, Schmid & Partner Engineering AG (SPEAG).
21. Y.W. Chi and K.L. Wong, Compact multiband folded loop chip antenna for small-size mobile phone, IEEE Trans Antennas Propag 56 (2008), 3797–3803.
22. T. Yang, W.A. Davis, W.L. Stutzman, and M.C. Huynh, Cellular-phone and hearing-aid interaction: An antenna solution, IEEE Antennas Propag Mag 50 (2008), 51–65.
23. K.L. Wong and M.F. Tu, Hearing aid-compatible internal penta-band antenna for clamshell mobile phone, Microwave Opt Technol Lett 51 (2009), 1408–1413.
24. C.H. Chang and K.L. Wong, Printed λ/8-PIFA for penta-band WWAN operation in the mobile phone, IEEE Trans Antennas Propag 57 (2009), 1373–1381.

DIFFRACTIVE OPTICAL ELEMENTS WITH SQUARE CONCENTRIC RINGS OF EQUAL WIDTH

Javier Alda,[1] Luis Miguel Sanchez-Brea,[2] Francisco Javier Salgado-Remacha,[2] and José María Rico-García[2]*

[1] Applied Optics Complutense Group, Optics Department, School of Optics, University Complutense of Madrid, Ave. Arcos del Jalón 118, 28037 Madrid, Spain; Corresponding author: j.alda@opt.ucm.es

[2] Physics Faculty, University Complutense of Madrid, Av Complutense s/n, 28040 Madrid, Spain

Received 25 June 2009

ABSTRACT: *A diffractive optical element having equal-width concentric square rings is analyzed in this article. This constant width makes possible its realization using spatial light modulators or square pixels phase screens. It allows a simple analytical treatment, and the element is also simulated using the Rayleigh-Sommerfeld approach. An experimental verification of its performance has been compared with the simulated results.* © 2010 Wiley Periodicals, Inc. Microwave Opt Technol Lett 52: 930–934, 2010; Published online in Wiley InterScience (www.interscience.wiley.com). DOI 10.1002/mop.25065

Key words: *diffractive optics; Fresnel zone plates; spatial light modulator*

1. INTRODUCTION

A Fresnel zone plate (FZP) is a diffractive element that is able to be integrated in microoptical devices. Its performance is based on the interference of successive zones, which are typically arranged following a phase-shift pattern, the Fresnel zones being the simplest solution [1]. The typical design for a FZP has circular shape zones and circular symmetry, like a refractive lens. However, it can be adapted to some other conformal geometries and off-axis operation [2]. These zones are also known as semiperiodic zones because the phase of the total amplitude arriving to the image point from the location of a given zone is shifted in π with respect to the phase coming from the adjacent zones. An alternative to a circular zone plate is a polygonal Fresnel zone plate [3]. When the number of sides of the polygon is low, the balance between the high focusing performance of a circular zone plate and the easiness of fabrication at micro and nanoscales of polygons represents a high advantage for the polygonal designs. The simplest polygonal shape is a triangle; however, the square because of its natural fitting to the rectangular coordinate system has deserved special attention [3, 4]. The design of a square Fresnel zone plates (SFZP) optimizes it to perform as a circular Fresnel zone plate. In a previous work [5], we have studied a SFZP design that is based on the minimization of the difference between the area covered by the angular sector of the zone of the corresponding circular plate and the one covered by the polygon traced on the plate. In the present contribution, we propose an alternative design for SFZP. In this case, the distance between the borders of consecutive zones is

*José María Rico-Garcia is currently at Centre de Recherche Paul Pascal, Bourdeax, France.